PERGAMON

Corrosion Science 44 (2002) 1027–1045

CORROSION SCIENCE

www.elsevier.com/locate/corsci

Electrochemistry of passive metals modified by manganese oxides deposited by *Leptothrix discophora*: two-step model verified by ToF-SIMS

Xianming Shi [a], Recep Avci [b], Zbigniew Lewandowski [a,c,*]

[a] *Department of Civil Engineering, Montana State University, Bozeman, MT 59717-3980, USA*
[b] *Department of Physics, Image and Chemical Analysis Laboratory, Montana State University, Bozeman, MT 59717-3980, USA*
[c] *Center for Biofilm Engineering, EPS Building, Room 314, Montana State University, Bozeman, MT 59717-3980, USA*

Received 5 February 2001; accepted 31 May 2001

Abstract

We have applied time-of-flight secondary ion mass spectroscopy (ToF-SIMS) to study microbially induced ennoblement of 316L stainless steel and Ti–6Al–4V surfaces exposed to manganese-oxidizing bacteria *Leptothrix discophora* SP-6. Our observations indicate that manganese biomineralization occurs in two steps: first, the divalent manganese (Mn^{2+}) is oxidized to manganese oxyhydroxide, MnOOH; then the MnOOH is further oxidized to manganese dioxide, MnO_2. Both reactions contribute to an increase in the open circuit potential and hence to the ennoblement of the material. Manganese cycling at a surface of passive metals produces renewable cathodic reactants, manganese oxyhydroxide and manganese dioxide, and endangers the material integrity.

Keywords: Time-of-flight secondary ion mass spectroscopy; Manganese-oxidizing bacteria; Ennoblement; Biomineralization

* Corresponding author. Address: Center for Biofilm Engineering, EPS Building, Room 314, Montana State University, Bozeman, MT 59717-3980, USA. Tel.: +1-406-994-5915; fax: +1-406-994-6098.
E-mail address: zl@erc.montana.edu (Z. Lewandowski).

0010-938X/02/$ - see front matter
PII: S0010-938X(01)00104-4

1. Introduction

As demonstrated by numerous authors, the microbial colonization of passive metals increases their open circuit potential (OCP) to final values between +200 mV_{SCE} [1] and +450 mV_{SCE} [2,3] through a series of reactions collectively termed ennoblement. This increase in OCP is associated with an increase in cathodic current density upon mild polarization [4]. Elevating OCP endangers the material integrity because, if raised high enough, the potential may approach the critical pitting potential of the passive metal and thereby increase the risk of localized corrosion. This occurrence is particularly likely when the metal is exposed to seawater.

Revealing the chemical and biological principles of ennoblement is thus as important for practical reasons as it is interesting as an illustration of how microbes modify the electrochemistry of metals. Determining the mechanism of ennoblement has also become an important area of study to those interested in microbially influenced corrosion, as ennoblement relates the effects of microbial action to easily measurable and well-defined electrochemical parameters: OCP and polarization currents.

Initial studies have explained ennoblement by a wide variety of mechanisms: microbially generated protons near the surface [5]; microbially generated hydrogen peroxide, possibly combined with low pH [6]; microbially produced organometallic catalysts of oxygen reduction [1,3]; specific enzymes [7]; and passivating siderophores [8]. The proposed mechanisms of ennoblement have been largely based on speculation of what can possibly cause the observed thermodynamic effect, the potential increase, and the kinetic effect, the increase in cathodic current density upon mild polarization of the ennobled metals.

More recent studies have linked the ennoblement of passive metals with the activity of manganese-oxidizing bacteria (MOB). For example, in the pitting corrosion reported by Linhardt [9,10], turbine runner blades (CrNi134) in a hydroelectric power plant in the Netherlands were found to be severely damaged despite being made of material resistant to the environmental chloride (20–170 mg/l), the most prevalent corrosion agent for that area. The observed behavior was thus thought to be a consequence of ennoblement. SEM/EDAX and X-ray diffraction analyses of deposits from the corroded blades revealed the presence of manganese-containing minerals (approximately 25 wt.% MnOOH and 8 wt.% MnO_2), which were suggested to be responsible for the massive pitting corrosion. Linhardt concluded that the elevated OCP (+570 mV_{SHE} = +330 mV_{SCE}) of the biological deposits scraped from the blades was due to the half-reaction described by reaction (1), the reduction of manganese dioxide to divalent manganese with a reduction potential of +550 mV_{SHE} at pH 7.5, $[Mn^{2+}] = 0.1$ mg/l.

$$MnO_2 + 4H^+ + 2e^- \rightarrow Mn^{2+} + 2H_2O \qquad E_0' = +550\ mV_{SHE} = +310\ mV_{SCE} \tag{1}$$

In our laboratory, Dickinson et al. [11] demonstrated that the OCP of 316L stainless steel reached +350 mV_{SCE} after a 30-day in situ exposure to a freshwater creek. He also found evidence that the microbial deposits formed characteristic rings,

identified as the diagnostic feature of a certain manganese-oxidizing bacterium, *Siderocapsa*. To demonstrate that the ennoblement was indeed caused by the MOB, Dickinson exposed corrosion coupons of 316L stainless steel to a batch culture of MOB, *Leptothrix discophora* SP-6, in a mineral–salt–pyruvate–vitamin medium containing divalent manganese. The coupons ennobled under these well-defined laboratory conditions and exhibited similar electrochemical properties to those ennobled in natural waters [12]. On the basis of this and some previous studies, Dickinson and Lewandowski [13] and Olesen et al. [14] concluded that the biomineralized manganese oxides on the stainless steel surface were responsible for the observed electrochemical behavior of the metal and suggested that the reaction controlling the process was the same as that in alkaline batteries:

$$MnO_2 + H_2O + e^- \rightarrow MnOOH + OH^- \qquad E_0' = +382\ mV_{SCE} \tag{2}$$

Recently in our laboratory, Olesen et al. [14,15] used X-ray photoelectron spectroscopy (XPS) to determine the chemical composition of microbial deposits on 316L stainless steel ennobled by biofilms of *Leptothrix discophora* SP-6 under laboratory conditions and to verify the mechanism of ennoblement suggested by Dickinson et al. [4,13]. Olesen determined the chemical composition of the deposits by comparing the Mn3p peak in the XPS spectra of the deposits with that in the reference spectra of different manganese oxides, and he concluded that the biologically deposited mineral was manganese dioxide. He also demonstrated that the biomineralized manganese dioxide was electrochemically reduced to divalent manganese via manganese oxyhydroxide, MnOOH. This mechanism differs from that proposed by Dickinson et al. [4,13] and from that proposed by Linhardt [9,10] because it proposes that the MnOOH is an intermediate product of the electrochemical reduction. If it were found that the final product of the cathodic reaction was divalent manganese, instead of MnOOH, then this process might have interesting implications for corrosion: since the divalent manganese ions are produced within biofilms containing MOB, the MOB could re-oxidize them back to manganese dioxide, therefore forming a renewable cathodic reactant. Such a scenario, if verified experimentally, could be quite dangerous for the material integrity because (1) the cathodic reactant is recyclable, (2) it is in solid state, so that its activity does not change as the reaction progresses, and (3) the supply of manganese oxides is not limited by the mass transport since they are deposited on the surface.

Although Dickinson et al. [4,12,13], Linhardt [9,10], and Olesen et al. [14,15] demonstrated that the microbial deposition of manganese oxides changes the electrochemical behavior of stainless steels, the chemical composition of the biomineralized manganese and the exact mechanism of ennoblement remain controversial. Based on the observation that the position and width for the Mn3p peak of MnO_2 is very close to that of MnOOH [14,15], and that both oxides are assumed in the mechanism, it is desirable to use surface analysis techniques other than XPS to verify the chemistry of the biomineralized manganese and, specifically, to distinguish MnOOH from MnO_2. To evaluate the effect of biomineralized manganese oxides on the localized pitting corrosion, it is also important to map the spatial distribution of the manganese deposits on metal surfaces and, further, compare this distribution

with the distribution of corrosion pits. XPS does not have adequate spatial resolution to provide such information either. Therefore, we decided to explore the capabilities of chemical imaging offered by time-of-flight secondary ion mass spectroscopy (ToF-SIMS) with the goal of determining the composition of biomineralized deposits and describing their spatial distribution on the metal surface.

ToF-SIMS offers high detection sensitivity and chemical imaging, can detect elements as well as chemical compounds, can differentiate among isotopes [16,17], and allows mass imaging with submicron spatial resolution [18]. Using computerized data collection and retrospective analysis, the two-dimensional imaging of spatial distribution of chemical composition is possible. Imaging SIMS has found application in the study of the mechanism of oxide growth. For example, the distribution of ^{18}O, Fe and Cr in an oxide scale grown on 9% Cr/Fe steel was obtained and found informative in understanding the corrosion mechanisms [16], and depth profiling of oxide layers was done to investigate a corroded zircaloy fuel rod cladding specimen [19]. In a recent SIMS application, the ratios MO_2^-/MO^- and MO_3^-/MO^- for transition metal oxides of the type M_xO_y were measured to identify their oxidation state. The data for iron oxide were then compared to those for the oxide found on a steel sample with an oxide film 4 nm thick, and the best match was to Fe_2O_3 [18].

We attempted to verify the mechanism of ennoblement caused by biodeposited manganese oxides by determining the chemical composition of microbial deposits on stainless steel coupons. However, the presence of alloying elements in the metal surface, especially iron and manganese, interfere with the Mn related secondary ion peaks in the SIMS spectra of microbial deposits on the ennobled coupons. For example, MnH^+ generated by microbial deposits and the metal substratum cannot be differentiated from Fe^+ generated by the metal substratum. The extent of this interference is unknown because we do not have an independent standard without these contributions. To alleviate this problem we used two types of coupons, 316L stainless steel and low-iron titanium alloy (Ti–6Al–4V), and exposed them to the same environments. Tables 1 and 2 give the elemental compositions of both alloys. Assuming that the chemical nature of the deposits is the same on both coupons in terms of manganese oxides, any differences in the SIMS spectra would reflect the effect of iron within the stainless steel coupons. Following this strategy, the SIMS spectra of the deposits on the Ti–6Al–4V coupons were used to verify the information obtained from the 316L stainless steel coupons.

Table 1
Elemental composition (wt.%) of 316L stainless steel corrosion coupons

Fe	Cr	Ni	Mo	Mn	Si	P	N	C	S
Bal.	16.19	10.19	2.10	1.71	0.39	0.034	0.03	0.017	0.001

Table 2
Elemental composition (wt.%) of Ti–6Al–4V corrosion coupons

Ti	Al	V	N	C	H	Fe	Mn	O
Bal.	6.0	4.0	0.05	0.1	0.012	0.3	0.01	0.2

Pure-culture biofilms of MOB were grown on corrosion coupons made of 316L stainless steel or Ti–6Al–4V under laboratory conditions. The composition of the microbial deposits was determined by comparing the positive/negative ion SIMS spectra of the deposits with the spectra of several manganese standards: MnO_2, MnOOH, Mn_3O_4, $MnCO_3$, MnO, and Mn_2O_3. We identified the manganese oxides on the ennobled metal samples and determined their spatial distribution.

2. Materials and methods

2.1. Metal samples and reactor

To make corrosion coupons, each 1.6 cm in diameter, we used two substrata: (1) 316L stainless steel and (2) Ti–6Al–4V. Both materials were cut from larger sheets provided by Metal Samples, Inc. (Munford, AL). Tables 1 and 2 show the composition of these materials, as provided by the vendor. Before the coupons were mounted in the holder, they were polished to provide a surface sufficiently devoid of flaws for the surface analysis. They were wet-sanded with tap water on Buehler-Met II metallographic grinding discs, composed of silicon carbide grit of decreasing grit sizes: 120, 240, 360, 400, and 600. After sanding at each grit size, the holder and coupon were rinsed with running tap water to remove any remaining grit. We then polished the coupons using Buehler aluminum oxide powder and Buehler Micropolish II powder, each suspended in water and applied to Buehler microcloths. We initiated polishing of the coupons with 5 μm aluminum oxide powder and then rinsed the coupons with tap water. In a similar manner we used 0.5 and 0.05 μm polishing powders to produce a mirror finish on the surface, with rinses applied after polishing with each powder size. The last step in cleaning the surface was to sonicate the coupons, first in acetone, then in 95% ethanol, for 5 min in each solvent. The coupons were then mounted in polycarbonate holders using a 100% silicone sealant (from Ace Hardware Co.) and electrically connected by fixing conductive springs to the unexposed side (Fig. 1).

The reactor was a polycarbonate batch cylinder reactor (Fig. 2), 10.2 cm tall and 11.1 cm in diameter, the same as that used by Olesen et al. [15]. Eight polished coupons were mounted to their holders, which were attached to the top of the reactor. Glass tubes were mounted in the reactor to aerate the growth medium. Pall-Gelman bacterial air vents were attached to these tubes to prevent contamination of the reactor. A magnetic stir bar, placed at the bottom of the reactor, provided stirring. The reactor was then sealed with silicon gel and autoclaved on the dry setting (depressurization method) at 123°C and 1.2 atm for 30 min.

2.2. Laboratory procedures

To grow the MOB we prepared 1 l of American Type Culture Collection (ATCC) culture medium 1917 MSPV (Table 3). The nutrient solution was autoclaved on the

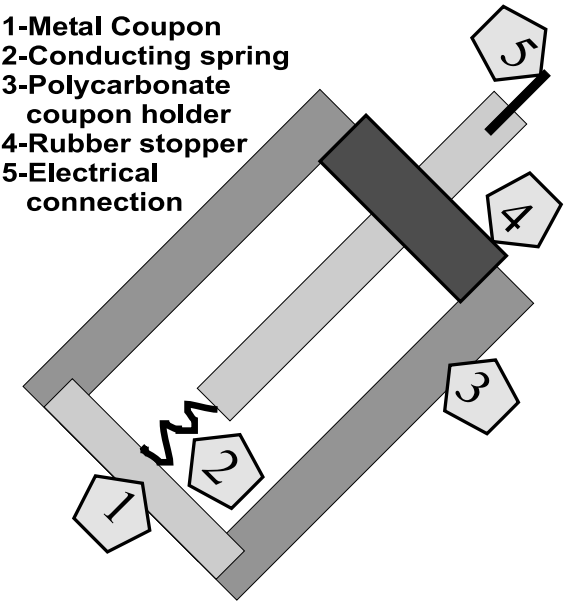

Fig. 1. The assembled coupon holder: the coupon (1) was mounted in the polycarbonate holder (3) using a 100% silicone sealant and electrically connected by fixing a conductive spring (2) to the unexposed side of the coupon. The top of the holder was protected with a rubber stopper (4), through which the electrical connection was established (5).

liquid setting at 123°C and 1.2 atm for 25 min. After the solution was cooled to room temperature, we aseptically added 1 ml of filter-sterilized vitamin solution, as required by the MSPV medium [20], 4 ml of filter-sterilized 50 mM manganese sulfate solution, and 5 ml of filter-sterilized 20% sodium pyruvate solution. All chemicals were from Fisher Scientific.

MOB, *Leptothrix discophora* SP-6 (ATCC 51168), were obtained from ATCC and stored at −70°C. To inoculate the reactor, we poured 150 ml of the MSPV medium with vitamins, sodium pyruvate, and manganese sulfate into a sterile 250 ml Erlenmeyer flask already holding the stock culture of the bacteria. The flask was placed on a shaker for 2 days, and then the culture broth was aseptically mixed with 600 ml of the sterile medium and added to the reactor.

The coupon assembly and reference electrode were connected to a computer via a Hewlett Packard 34970A Data Acquisition/Switch Unit (a 20-channel armature multiplexer) to monitor the OCPs of the coupons. The SCE reference electrode was sterilized by soaking it in 99% ethanol for 1 h. Prior to inoculating the reactor with *Leptothrix discophora*, the coupons were immersed in the culture medium for 48 h to make sure that the OCPs were stabilized. The reactor was operated until the potentials of the coupons stabilized at over +350 mV_{SCE}, which, according to our definition, indicated that the coupons were *fully ennobled*. Using these experimental procedures, it took about 80 h to ennoble the coupons (Fig. 3).

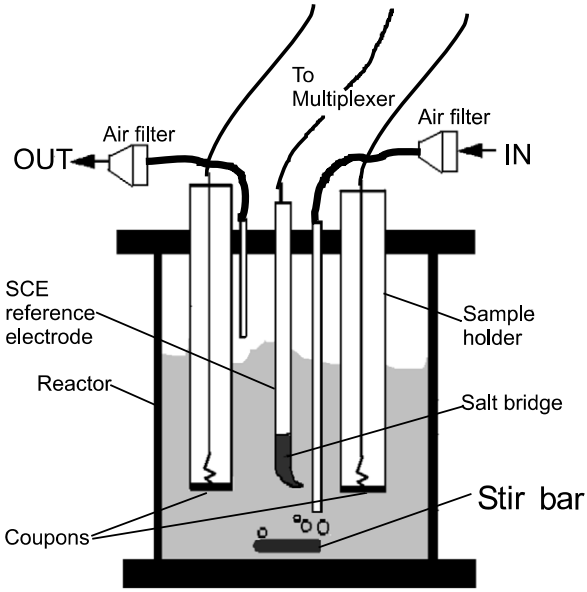

Fig. 2. The reactor we used to grow the manganese-oxidizing microorganisms and to ennoble the coupons. During a typical run we used eight polycarbonate holders (Fig. 1) with polished coupons. The OCPs of the coupons were measured against a reference electrode every 30 min using a multiplexer interfaced with a computer.

Table 3
The components and preparation[a] of ATCC culture medium 1917 MSPV for *Leptothrix discophora*

$(NH_4)_2SO_4$ (g)	$MgSO_4 \cdot 7H_2O$ (g)	$CaCl_2 \cdot 2H_2O$ (g)	KH_2PO_4 (g)	$Na_2HPO_4 \cdot 7H_2O$ (g)	HEPES (g)	10 mM $FeSO_4$ (ml)
0.24	0.06	0.06	0.02	0.05	2.383	1.0

[a] Add distilled water to 984 ml, adjust to pH 7.2 by adding either NaOH or H_2SO_4.

2.3. Time-of-flight secondary ion mass spectroscopy analyses

When the sample surface of a metal in vacuum is bombarded by 15–25 keV energetic particles (referred to as the *primary ion beam*), various atomic or molecular low-energy particles are emitted (a process known as *sputtering*). The total number of primary ions per unit area is kept below the static SIMS limit ($< 10^{13}$ cm^{-2}). A small percentage of the sputtered species are ionized naturally (*secondary ions*) and may be extracted by an electric field and transferred into a mass spectrometer, where the mass-to-charge ratios are separated. In ToF-SIMS instruments, the sample is bombarded by the pulsed primary ion beam for only a very short period of time (ns range). In the time between two successive pulses ($\sim$100 μs), the generated secondary ions are post-accelerated in a flight tube and then mass separated according to the exact flight time to reach the detector. Secondary ions with different mass-to-charge

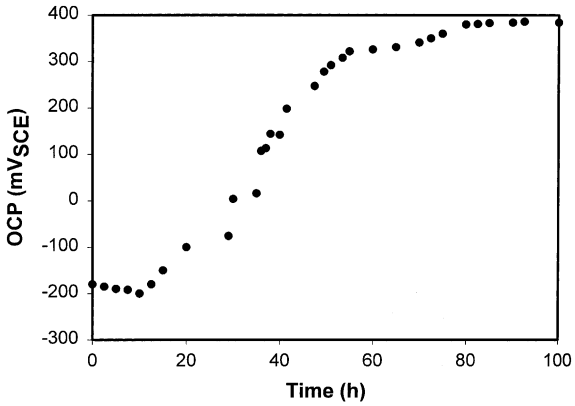

Fig. 3. A typical temporal evolution of the OCP of a 316L stainless steel coupon exposed to MOB in the reactor shown in Fig. 2. The OCP finally stabilized at around +380 mV_{SCE}, which indicates that the coupon was fully ennobled. The Ti–6Al–4V coupons showed a similar OCP evolution.

ratios are then identified, and the cumulative (typically 5 min acquisition time) ion counts for each mass are recorded. Typically less than 1% of the total sample surface is removed by the bombardment during data acquisition. A surface mass spectrum, secondary ion count vs. mass-to-charge ratio (m/z), is thus obtained, in which the mixture of elemental and cluster ions can generate a rich set of information about the chemistry of the virgin surface layer.

We used a Phi-Evans TRIFT I ToF-SIMS [17] with a pulsed gallium liquid metal ion gun fired at 25 keV primary energy (corresponding to 22 keV impact energy), with a 10 kHz repetition rate, as the primary beam source. A multi-stop time-to-digital converter recorded the time of flight of the ion fragments with a 138 ps precision. The TRIFT I LMIG provides <1 μm spatial resolution while simultaneously detecting ion fragments with $\sim m/\Delta m \sim 2000$ mass resolution. A raster area of 80×80 μm^2 was chosen as the X–Y image field, and the LMIG pulse width was adjusted (<14 ns) to give a maximum secondary ion intensity in the range of $0.3 \times 10^4 - 1.0 \times 10^4$ counts/s during data acquisition.

In all of the ToF-SIMS acquisitions we stayed within the limit of static SIMS requirements, which means the primary ion dose remained below 10^{13} ions/cm^2. A beam of low-energy (<20 eV) electrons was fired intermittently to prevent charging of the sample. The data acquisition and analysis were done using both DOS and Win-Cadence ToF-SIMS software (physical electronics).

2.3.1. Samples for SIMS analyses

Six manganese oxides were used as standards to collect their ToF-SIMS reference spectra (positive and negative ions). We chose MnO_2, MnOOH, Mn_3O_4, and $MnCO_3$ because they are the predominant species of manganese oxides in natural waters [15]. In addition, we chose MnO and Mn_2O_3 to include other oxidation states of manganese that could be present on the ennobled coupons. Five of the oxides

were commercial products from Aldrich Chemical Company, Inc.: MnO (99%), Mn_2O_3 (99%), MnO_2 (99%), Mn_3O_4 (97%) and $MnCO_3$ (99.9+%). The sixth was a natural sample of the mineral manganite (MnOOH) from Wards Natural Science Establishment, Inc. The sample of MnOOH was cut, fractured, and immediately inserted into the analysis chamber in vacuum to minimize surface contamination. From the X-ray powder diffraction patterns we verified that the sixth sample was pure manganite (δ-MnOOH) [21].

We prepared the manganese standards for SIMS analysis by gently pressing the powdered compounds into a piece of soft indium foil (Alfa, ESAR), using clean glass slides to ensure that the surface to be analyzed was flat. As a result, the sample spectra included a peak from indium, but this did not interfere with any peaks of importance for this study.

To analyze the surface chemistry of the ennobled coupons, we gently removed the biofilm using 95% ethanol, distilled water and a paper tissue. The coupons were then mechanically removed from the holders, air-dried and kept in separate airtight containers for up to 24 h prior to SIMS analysis to ensure dryness. After the SIMS analysis we carefully removed the deposits from each coupon using a paper tissue and distilled water and then collected the SIMS spectra of each coupon again. The latter results were used as controls, reflecting the chemistry of the bare metal surface.

2.3.2. Region-of-interest analysis

Since the microbial deposits were not uniformly distributed on the surface, we needed to eliminate the areas that were not covered by deposits and determine the composition of the deposits only. The raw data acquisition of ToF-SIMS stores a complete mass spectrum for each of the 256×256 pixels uniformly distributed through the area of interest. Retrospective analysis of the SIMS data makes it possible to obtain chemical maps of the specific ion fragments of our choice because each of the 256×256 pixels contains the full mass spectrum stored in the computer. To define the chemical composition of microbial deposits, we run what is known as "region-of-interest" (ROI) analysis during a retrospective analysis of "raw" data files [16]. An ROI was defined by using a simple drawing tool to select the areas in a SIMS image from which mass spectra were acquired. For example, when analyzing the surface of the titanium coupons, the Ti^+-depleted regions were defined as the ROIs from which positive ion spectra were collected (Fig. 5).

3. Results and discussion

3.1. Surface chemistry and the extent of ennoblement

Using the imaging capabilities of ToF-SIMS, we generated chemical maps of the spatial distribution of the secondary ions of interest on the surface of a fully ennobled Ti–6Al–4V coupon (OCP = 380 mV_{SCE}). Fig. 4 shows the distributions of Ti^+, Al^+ and Mn^+ on the Ti–6Al–4V coupon. Ti^+ and Al^+ are similarly distributed; Mn^+ is enriched in the regions where Ti^+ is depleted, and lacking in the Ti^+-rich

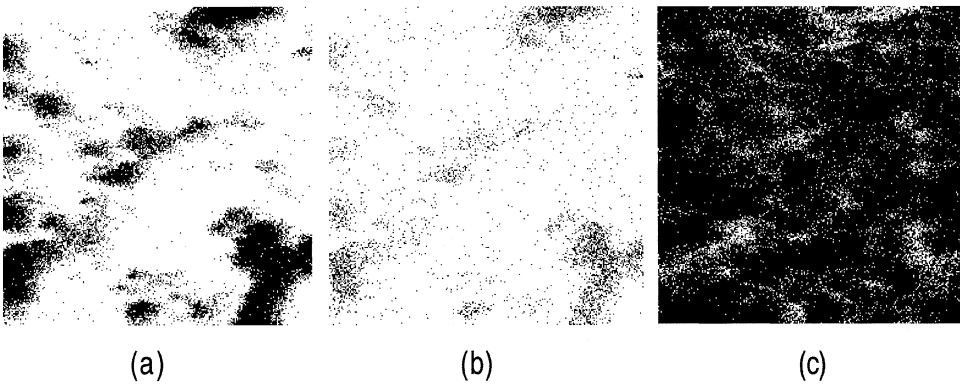

Fig. 4. ToF-SIMS images of an 80×80 μm^2 area of a fully ennobled Ti–6Al–4V coupon (OCP = +380 mV_{SCE}) show the distributions of secondary ions: (a) Ti^+; (b) Al^+; (c) Mn^+. The dark regions are enriched in (a) Ti^+, (b) Al^+ and (c) Mn^+. Ti^+ and Al^+ are similarly distributed, but Mn^+ is enriched in the regions where Ti^+ signal intensity is lower. This is an expected result if the Ti^+ and Al^+ signals are coming from the metal and the Mn^+ signal is coming from the deposits. Therefore, we hypothesize that the regions of increased manganese coincide with the biofilm-rich regions. The gray-scale intensity in all images corresponds to the intensity of the detected ions (the darker the image, the stronger the intensity of the secondary ion counts per unit area, or per pixel).

areas. Based on the results of this chemical mapping, we hypothesized that the zones covered with manganese coincided with the zones covered by the biofilm. Observations also indicated that the microbially deposited manganese was not chemically bonded with the titanium alloy substratum, which was further verified by XPS studies in our laboratory. The Ti^+-depleted regions on the titanium coupons, defined as ROIs, clearly show peaks of manganese compounds (Fig. 5).

To establish the relation between the surface chemistry and the degree of ennoblement, we analyzed the chemistry and spatial distribution of inorganic deposits on 316L stainless steel coupons ennobled to different OCP: (1) *non-ennobled* OCP ~ -200 mV_{SCE}; (2) *partly ennobled*, OCP = +270 mV_{SCE}; and (3) *fully ennobled*, OCP = +380 mV_{SCE}. The ToF-SIMS analyses show that as the ennoblement progresses, the total amount of manganese oxides deposited on the metal surface increases. Consequently, the surface of the coupon that is in immediate contact with the aqueous phase is changing in chemistry. Fig. 6 shows the elemental images (with micron bars showing length scale) of the distribution of Mn^+ and FeH^+ on 316L stainless steel coupons. (Fe^+ mapping is not used because it cannot be separated from that of MnH^+.) For the non-ennobled coupon, FeH^+ (1b) is uniformly enriched (black regions) while the image shows only traces of Mn^+, which is consistent with the chemical composition of 316L stainless steel. As the degree of ennoblement increases, Mn^+ appears more and more enriched in the regions where the FeH^+ signal is reduced. On the fully ennobled coupon, the FeH^+ ions are significantly reduced (white regions in 3b) while Mn^+ covers most of the surface area (dark regions in 3a), indicating that the surface film on the stainless steel sample is progressively enriched with manganese as the ennoblement process progresses. It is

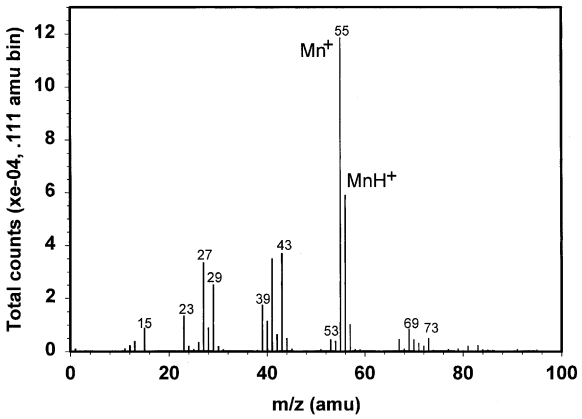

Fig. 5. Positive ion ToF-SIMS spectrum: secondary ion counts per ~0.1 amu-bin vs. mass-to-charge ratio (m/z 0–100 amu). The spectrum was collected retrospectively from the Ti^+-depleted regions (ROI) shown in Fig. 4a. These regions are Mn-rich on the *fully ennobled* Ti–6Al–4V sample (OCP = +380 mV_{SCE}). The SIMS spectrum shows secondary ion peaks due to manganese oxides, especially Mn^+ and MnH^+, which dominate the spectra. In the above spectrum the MnH^+ peak also contains some Fe^+ as evidenced by the FeH^+ peak at 57 amu. Based on the chemical mapping, we conclude that the source of Fe in this case is the $FeSO_4$ in the culture medium. The relative intensity of the secondary ions can be calculated in terms of counts, i.e., the areas under the peaks.

impressive that the surface sensitivity at submonolayer scale of the ToF-SIMS was able to differentiate the non-homogeneous distribution of Fe (represented by FeH^+) and Mn as a result of ennoblement. The matrix effects, usually the dominant effects in ToF-SIMS, play a secondary role in this interpretation.

3.2. Chemical composition of microbial deposits

For each manganese standard, several secondary ion species of different intensities were formed during the SIMS process: the most characteristic ones for positive ion spectra are Mn^+ and MnH^+ (see Fig. 5), while for the negative ion spectra they are MnO^- and $MnOH^-$. The typical SIMS mass spectrum provides a means for qualitatively identifying the chemical composition of a few atomic layers near the surface of the sample.

To identify and quantify various oxides and their observed differences, we used two groups of ratios of signal intensities as indicators: MnH^+/Mn^+ for the positive ion spectra, and $MnO^-/MnOH^-$ for the negative ion spectra. To achieve statistical reliability, we collected the SIMS spectra from five to seven different areas on each sample, including manganese standards and metal coupons, and then calculated the mean value and subsequently the standard deviation of the ratios using the procedure we developed as explained below.

The ratios of signal intensities from the manganese standards are shown in Table 4. These ratios appear to be characteristic for each oxidation state, which corroborates the conclusions of Benninghoven and coworkers [22] with respect to the

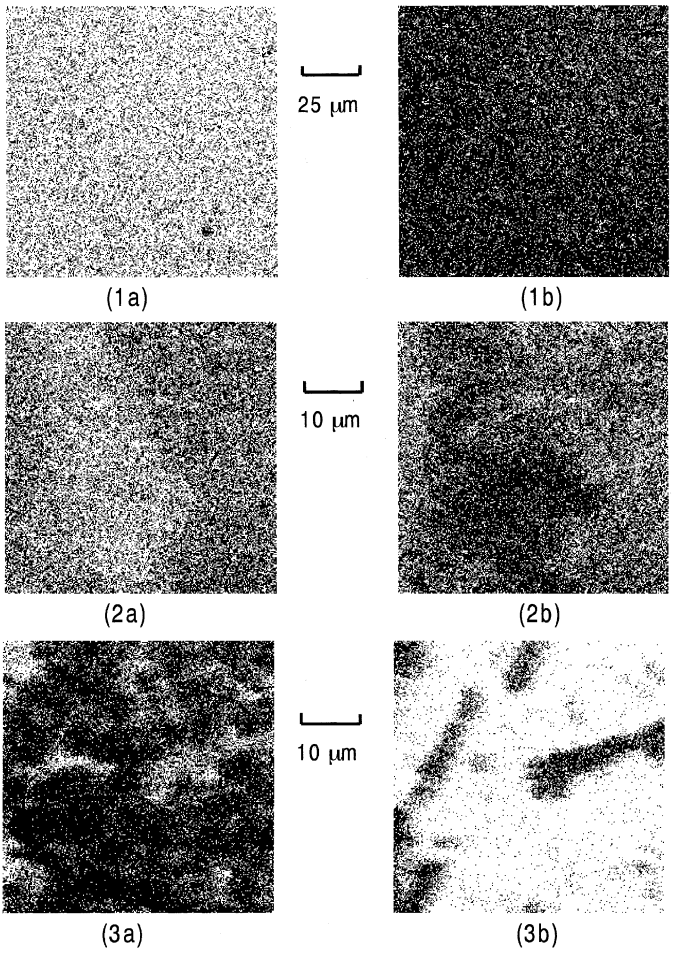

Fig. 6. ToF-SIMS images showing the distribution of secondary ions: (a) Mn^+ and (b) FeH^+. Data collected from 316L stainless steel samples: (1) *non-ennobled*, OCP ~ -200 mV_{SCE}; (2) *partly ennobled*, OCP $= +270$ mV_{SCE}; (3) *fully ennobled*, OCP $= +380$ mV_{SCE}. As the degree of ennoblement (assessed by the value of OCP) increases, the regions rich in Mn^+ grow while the regions rich in FeH^+ diminish. For the fully ennobled coupon, the areas rich in Fe^+ are significantly depleted (white regions in 3b) while the areas rich in Mn^+ are large (dark regions in 3a). As anticipated, this contrast indicates that the surface film on some regions of the stainless steel sample is progressively enriching with manganese as the ennoblement process progresses. In all images, the gray-scale intensity corresponds to the signal intensity. (The darker the image, the stronger the intensity of the secondary ion of interest.)

relative yields of $Me_yO_x^{\pm}$. Because there is a clear relationship between the ratios of signal intensities and the oxidation state of the oxides (as suggested by the standard deviations, which are at least an order of magnitude smaller than the mean values), the relative intensities of the secondary ions can be used to identify the oxidation state of each oxide. This process can be used to identify unknown manganese oxides in natural surfaces. For a mixture of manganese oxides, it is also possible to identify

Table 4
Relative intensity ratios of interest in the SIMS spectra of the selected manganese standards[a]

	MnO	Mn_2O_3	$MnCO_3$	Mn_3O_4	MnOOH	MnO_2
MnH^+/Mn^+						
Mean value	0.215	0.253	0.271	0.394	1.847	0.477
Standard deviation	0.019	0.023	0.002	0.003	0.056	0.006
$MnO^-/MnOH^-$						
Mean value	1.336	0.918	2.779	1.028	0.492	0.905
Standard deviation	0.097	0.012	0.244	0.078	0.079	0.083

[a] See also the bar chart shown in Fig. 7.

the mixed composition in a semi-quantitative manner by using the SIMS spectra of well-defined standards.

Table 4 shows that we can identify oxidation states of manganese oxides using the secondary ions in the positive and negative SIMS spectra. The data are reproducible within the range of acceptable experimental error. Because the intensity ratios were measured using the same instrumental parameters, these values can be considered as a measure of the variations from sample to sample and from location to location on a given sample.

In the SIMS analysis of the ennobled coupons, it was found that the signals of Mn^+ and Fe^+ (MnH^+) from the areas not covered with microbial deposits contribute to those from the inorganic microbial deposits that we aim to identify. To remove this interference, we collected SIMS spectra from the ennobled coupon and from the metal surface with microbial deposits removed. As described below, for every peak analyzed we subtracted the normalized counts reflecting the secondary ions from the metal substratum: the difference is the signal from the microbial deposits.

For 316L stainless steel, we used FeH^+ and FeH^- as internal intensity reference peaks and subtracted the normalized signals due to the substratum from the positive and negative SIMS counts to determine the counts due to the deposits. Similarly, for the Ti–6Al–4V we used TiH^+ and TiH^- as internal reference peaks for doing our subtraction. Below, we give an example of the typical procedure for determining the MnH^+/Mn^+ ratio.

Eq. (3) is the relation for subtracting counts, while Table 5 illustrates how the internal references were used for determining the true values of the counts due to Mn^+ and MnH^+. The basic idea behind the equation is that the FeH^+ does not have much contribution from manganese (because of the very low yield of MnH_2^+), whereas the MnH^+ comprises a substantial fraction of Mn^+ yield and MnH^+ cannot be differentiated from Fe^+.

$$[Me^+]_{deposits} = [Me^+]_{ennbl} - [FeH^+]_{ennbl} \times R_{Me^+/FeH^+} \quad (3)$$

In this formula: Me^+ stands for any of the Mn^+ or MnH^+ counts; $[Me^+]_{deposits}$ is the Me^+ counts from the microbial deposits (Table 5, columns 7 and 8); $[Me^+]_{ennbl}$ is the Me^+ counts from the ennobled coupon, including counts from the substratum

Table 5
An example of applying Eq. (3) to determine the ratio MnH^+/Mn^+ for five different areas of a fully ennobled 316L stainless steel coupon, SS-1 (ennobled to $+380\ mV_{SCE}$)[a]

Area	Mn^+	$(MnH^+ + Fe^+)$[b]	FeH^+	Mn^+/FeH^+	$(MnH^+ + Fe^+)$[b]$/FeH^+$	Mn^+	MnH^+	MnH^+/Mn^+
1	277 771	210 340	35 123	0.150	2.144	272 503	135 036	0.496
2	261 263	214 082	39 453	0.150	2.144	255 345	129 495	0.507
3	254 249	221 768	44 158	0.150	2.144	247 625	127 093	0.513
4	295 848	216 750	35 144	0.150	2.144	290 576	141 401	0.487
5	305 210	222 311	35 954	0.150	2.144	299 817	145 226	0.484

[a] Columns 2–4 show the counts (areas under the peaks) of Mn^+, $MnH^+ + Fe^+$, and FeH^+. Columns 5 and 6 show the mean intensity ratios for Mn^+/FeH^+ and $(MnH^+ + Fe^+)/FeH^+$ of the bare metal surface. Columns 7 and 8 show the true Mn^+ and MnH^+ counts. And column 9 shows the intensity ratio of MnH^+/Mn^+, which is used as a fingerprint for the oxidation state of each of the biomineralized manganese oxides. The mean value of MnH^+/Mn^+ is 0.497 and the standard deviation is 0.013.

[b] The two peaks cannot be resolved.

surface and from the deposits (Table 5, columns 2 and 3); and $[FeH^+]_{ennbl}$ is the FeH^+ counts from the ennobled coupon (column 4). R_{Me^+/FeH^+} is the mean value of the intensity ratio Me^+/FeH^+ of the bare metal surface only (Table 5, columns 5 and 6). These values are then used in relation to Eq. (3) to determine the true ratio of MnH^+/Mn^+ (Table 5, column 9). With this ratio we can identify the oxidation state of biomineralized manganese oxides.

Fig. 7 shows the intensity ratios of the secondary ions of interest in the SIMS spectra of a fully ennobled Ti–6Al–4V (Ti-1), a fully ennobled 316L stainless steel (SS-1), and two partially ennobled 316L stainless steel (SS-2, SS-3) coupons, together with the manganese oxide standards. The OCPs of the metal coupons, measured just before they were taken out of the culture medium for surface analysis, are given in Table 6. The standard deviation of the intensity ratios relative to the mean values varies from 0.4% to 21.1%.

One reason for some of the high standard deviations may be the fact that the exact chemical composition of microbial deposits can vary on a micron scale on the same surface of an ennobled metal sample. They can also be partly explained by variations in the matrix effects. Since obtaining surfaces sufficiently free of organic contamination is difficult, the presence of organics may affect the secondary ion species associated with the generation of inorganic species. XPS depth profile studies of these oxide films by other members of our group confirm the presence of organic species in these films. In spite of such difficulties, the ToF-SIMS fragmentation patterns of manganese standards are of great diagnostic value, and the variation of inorganic microbial deposits on the metal samples can be probed with reasonable confidence and accuracy.

The intensity ratios in the SIMS data can be used to identify the oxidation state of manganese oxides. As shown in Fig. 7a, the mean ratios of MnH^+/Mn^+ (0.497 and 0.498) in the SIMS spectra of microbial deposits on fully ennobled Ti–6Al–4V and 316L stainless steel coupons are very close to that of the manganese dioxide standard (0.477). The results indicate that the inorganic microbial deposits on fully ennobled coupons, both stainless steel and titanium, are mainly composed of MnO_2. This

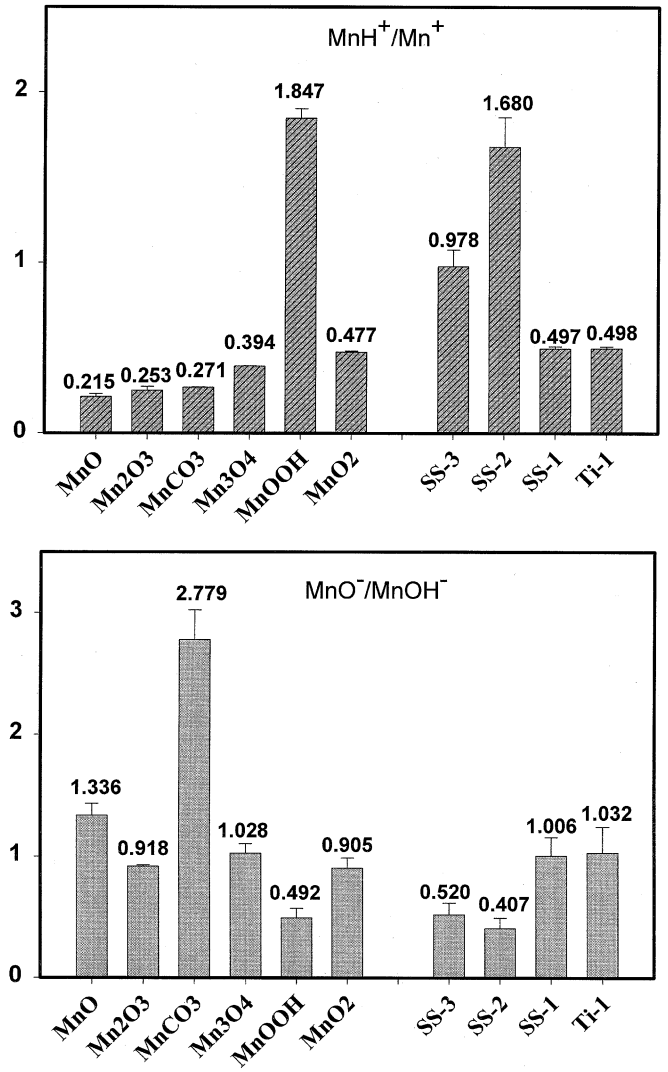

Fig. 7. Intensity ratios of secondary ions as a function of oxide standards and unknown oxide deposits on various coupons: (a) MnH^+/Mn^+ and (b) $MnO^-/MnOH^-$. The ratios MnH^+/Mn^+ and $MnO^-/MnOH^-$ in the SIMS spectra show that the biomineralized manganese on fully ennobled Ti–6Al–4V and 316L stainless steel coupons is mainly manganese dioxide. The same ratios on partly ennobled stainless steel coupons show that the deposits are mostly manganese oxyhydroxide (SS-2) or a mixture of manganese dioxide and manganese oxyhydroxide (SS-3). The relative ratios in the spectra of microbial deposits from the fully ennobled Ti–6Al–4V (Ti-1) and 316L stainless steel coupons (SS-1) are very close, which confirms the assumption that the chemical nature of the manganese minerals is the same on both coupons and verifies that the subtraction method used for data analysis (as explained above) is reliable.

conclusion corroborates the conclusions of previous researchers [4,12,23] and indicates the subtraction method as described above for quantitative analysis is reliable.

Table 6
The OCP and surface chemistry of the metal coupons ennobled under laboratory conditions

	Ti-1	SS-1	SS-2	SS-3
OCP	+380 mV_{SCE}	+380 mV_{SCE}	+270 mV_{SCE}	+320 mV_{SCE}
Surface deposits	Mainly MnO_2	Mainly MnO_2	Mainly MnOOH	Mixture of MnOOH and MnO_2

In contrast, for the partly ennobled 316L stainless steel coupons the mean ratio of MnH^+/Mn^+ of microbial deposits is very close to that of the manganese oxyhydroxide standard (for SS-2, 1.680) or remains between those of manganese dioxide and manganese oxyhydroxide (for SS-3, 0.978). The novel finding is that the microbial deposits on the partly ennobled stainless steel coupons are composed either of MnOOH (for SS-2) or a mixture of MnO_2 and MnOOH (for SS-3). This is different from the previous model [14,15], which suggested that the deposits should be entirely composed of MnO_2. The amount of other manganese oxides, such as Mn_3O_4 and $MnCO_3$, is negligible. The ratios of $MnO^-/MnOH^-$, as shown in Fig. 7b, also confirm these findings.

Based on our observations, we conclude that the microbial deposits on partly ennobled samples are composed of a mixture of MnOOH and MnO_2, and that those on fully ennobled samples are composed of MnO_2. As the ennoblement process progresses, the oxidation state of biomineralized manganese gradually evolves from +3 to +4, i.e., from MnOOH to MnO_2, as indicated in Table 6. This observation suggests that the MnOOH we identified with SIMS on the passive metal surfaces be due to the microbial oxidation of Mn^{2+}, instead of the electrochemical reduction of MnO_2 (see Fig. 8). Therefore, the mechanism of ennoblement we proposed in the previous papers [14,15] must be modified.

First, the biological oxidation of divalent manganese ions to manganese dioxide has an intermediate product, manganese oxyhydroxide, MnOOH. In previous papers we demonstrated that the same compound is an intermediate product during the reduction of manganese dioxide to divalent manganese [14,15]. In light of our present data, the manganese oxyhydroxide detected on ennobled metal samples may not entirely be a product of electrochemical reduction of MnO_2 – it can also be a product of microbial oxidation of divalent manganese.

Our observations suggest that the ennoblement occurs in two steps:

(1) Divalent manganese ions are oxidized to manganese oxyhydroxide in reaction (4), which has a reduction potential of +199 mV_{SCE} at pH = 7.2, $[Mn^{2+}] = 0.2$ mM. The experimental OCP of the *partly ennobled* coupon (SS-2), +270 mV_{SCE}, was a little higher than the theoretical value we anticipated. This discrepancy may be explained by the fact that part of the manganese oxyhydroxide had already been oxidized to manganese dioxide as suggested by the ratio of MnH^+/Mn^+ in the SIMS spectra (Fig. 7).

(2) Manganese oxyhydroxide is further oxidized to manganese dioxide as described in reaction (5), which has a reduction potential of +382 mV_{SCE} at pH = 7.2 and resulted in the elevated OCP of *fully ennobled* coupons at +380 mV_{SCE}.

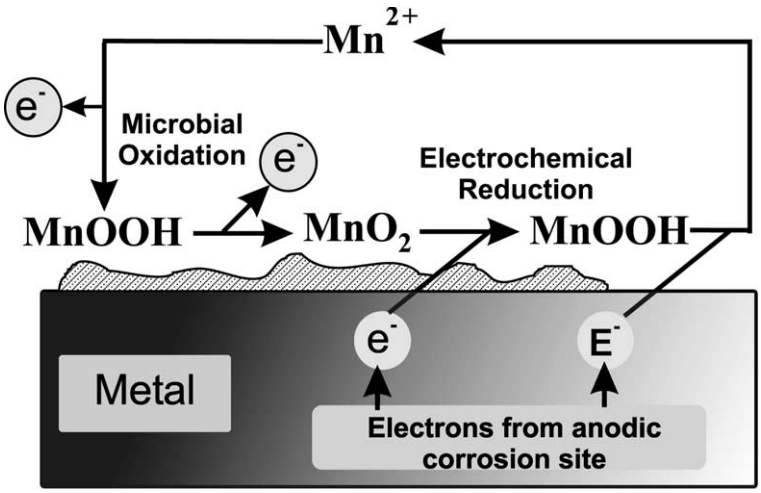

Fig. 8. Manganese cycling at a surface of passive metals includes biomineralization of divalent manganese and electrochemical reduction of manganese oxides. Manganese oxides are reduced to divalent manganese, which is, again, microbially re-oxidized. This sequence of events, called ''manganese cycling on metal surfaces'', produces renewable cathodic reactants, manganese oxyhydroxide and manganese oxide, and endangers the material integrity.

This evolution of manganese oxides from MnOOH to MnO_2 explains the electrochemical processes responsible for the OCP values measured during the ennoblement. The OCP of the metal coupons increased gradually and finally reached a plateau as the ennoblement process progressed. This observation is consistent with the two-step mechanism shown above, where the amount of MnOOH relative to MnO_2 plays a significant role.

$$Mn^{2+} + 2H_2O \rightarrow MnOOH + 3H^+ + e^- \qquad E^0 = 1.500\ V_{SHE} \tag{4}$$

$$MnOOH \rightarrow MnO_2 + H^+ + e^- \qquad E^0 = 1.050\ V_{SHE} \tag{5}$$

Fig. 8 shows the modified representation of the manganese cycle at surfaces of passive metals: biomineralization of manganese and electrochemical reduction of deposited oxides. The overall conclusion about the role of manganese oxides as renewable cathodic reactants is similar to that proposed in the previous papers from our laboratory [15]. However, our present study identified a new intermediate product, manganese oxyhydroxide, during oxidation of manganese. Incidentally, this is the same oxide that was identified previously [15] as an intermediate product in the reduction stage of the cycle. This finding may be supported by the results presented by Linhart [9,10], who found significant amounts of MnOOH in the biological deposits (approximately 25 wt.%) on the surface of corroding turbine blades.

We know that in natural waters manganese oxides deposited on metal surfaces tend to be electrochemically reduced to lower and thus more stable oxidation states. That is, MnO_2 tends to be reduced to MnOOH, and MnOOH tends to be further

reduced to divalent manganese. Based on the two-step biomineralization mechanism, the absolute amounts of manganese oxyhydroxide and manganese dioxide, and their respective ratio are dependent on the rates of biological oxidation and electrochemical reduction. The ratio of these two oxides on ennobled metal surfaces may vary depending on the rates of biological oxidation and electrochemical oxidation, two pathways of the proposed mechanism, and account for the observed electrochemical behavior of microbially colonized passive metals.

Using ToF-SIMS to identify the chemical composition of metal oxides and their spatial distribution on metal surfaces is a novel approach. In our case, the ability to determine mass spectra, combined with the high spatial resolution and imaging capabilities of the ToF-SIMS technique, allowed us to identify the manganese oxides and determine their location on the surface of passive metal coupons. The chemical maps collected by ToF-SIMS, e.g., Figs. 4 and 6, indicate that the manganese minerals were not uniformly deposited on the surface of the metals. The spatial distribution of biomineralized manganese might be further compared to that of corrosion pits generated by immersing the ennobled coupons into chloride solutions. We expect that this comparison may provide decisive information leading to the determination of how pitting is initiated on microbially colonized passive metals, which is the subject of our ongoing research. In general, applying ToF-SIMS to identify oxides and their spatial distribution on metal surfaces has great potential for corrosion research.

Finally, our results describe the mechanism of ennoblement in laboratory conditions using a pure culture of MOB and well-defined water chemistry. This mechanism may be more complex in natural environments where more than one type of microorganism may be able to biomineralize manganese, and minerals other than manganese oxides may also be microbially deposited.

4. Conclusions

- Manganese oxides deposited by the MOB *Leptothrix discophora* SP-6 on 316L stainless steel corrosion coupons consisted of manganese oxyhydroxide (MnOOH) and manganese dioxide (MnO_2). The verified mechanism suggests that the manganese biomineralization occurred in two steps: first, the divalent manganese (Mn^{2+}) was oxidized to manganese oxyhydroxide, MnOOH; then the MnOOH was further oxidized to manganese dioxide, MnO_2. Both reactions contributed to an increase in OCP.
- ToF-SIMS was successfully used to identify the biomineralized manganese oxides on ennobled 316L stainless steel and on Ti–6Al–4V samples. A high mass resolution, coupled with the high spatial resolution capabilities of ToF-SIMS, allowed the identification of various Mn oxides and their spatial distribution on the surface.

Acknowledgements

This work was supported by United States Office of Naval Research, contract no. N00014-99-1-0701 and by Cooperative Agreement EEC-8907039 between the

National Science Foundation and Montana State University, Bozeman, MT, USA. We would also like to specially thank the ICAL facility of Montana State University for the use of the XPS and ToF-SIMS.

References

[1] R. Johnsen, E. Bardal, Corrosion 41 (5) (1985) 296–302.
[2] A. Mollica, A. Trevis, Correlation Entre la Formation de la Pellicule Primaire et la Modification de la Cathodique sur des Aciers Inoxydables Expérimentés en eau de Mer aux Vitesses de 0,3 A5, 2 m/s, in: Proceedings of 4th International Congress on Marine Corrosion and Fouling, Antibes, France, 1976.
[3] S. Motoda, Y. Suzuki, T. Shinohara, Corros. Sci. 31 (1990) 515.
[4] W.H. Dickinson, F. Caccavo Jr., Z. Lewandowski, Corros. Sci. 38 (8) (1996) 1407.
[5] S.C. Dexter, G.Y. Gao, Corrosion 44 (10) (1988) 717.
[6] P. Chandrasekaran, S.C. Dexter, Proceedings of Corrosion 1993, paper no. 493, Houston, TX, NACE, 1993.
[7] V. Scotto, R. DiCintio, G. Marcenaro, Corros. Sci. 25 (3) (1985) 185.
[8] M. Eashwar, S. Maruthamuthu, Biofouling 8 (1995) 203.
[9] P. Linhardt, Failure of chromium–nickel steel in a hydroelectric power plant by manganese-oxidizing bacteria, in: E. Heitz, H.-C. Flemming, W. Sand (Eds.), Microbially Influenced Corrosion of Materials, Springer, Berlin, 1996, pp. 221–230.
[10] P. Linhardt, Werkstoffe und Korrosion 45 (1994) 79.
[11] W. Dickinson, Z. Lewandowski, Proceedings of Corrosion 1995, paper no. 223, Houston, TX, NACE, 1995.
[12] W.H. Dickinson, F. Caccavo Jr., B.H. Olesen, Z. Lewandowski, Appl. Env. Microbiol. 63 (7) (1997) 2502.
[13] W.H. Dickinson, Z. Lewandowski, Biofouling 10 (13) (1996) 79.
[14] B.H. Olesen, R. Avci, Z. Lewandowski, Proceedings of Corrosion 1998, paper no. 275, Houston, TX, NACE, 1998.
[15] B.H. Olesen, R. Avci, Z. Lewandowski, Corros. Sci. 42 (2) (2000) 211.
[16] D. Briggs, A. Brown, J.C. Vickerman, Handbook of Static Secondary Ion Mass Spectrometry, Wiley, New York, 1990.
[17] N.M. Reed, J.C. Vickerman, Static SIMS – surface analysis of inorganic materials, in: D. Briggs, M.P. Seah (Eds.), Practical Surface Analysis, second ed., vol. 2 – Ion and Neutral Spectroscopy, Wiley, New York, 1996, pp. 303–366.
[18] S.S. Cristy, Secondary ion mass spectrometry, in: C.M. Barshick, D.C. Duckworth, D.H. Smith (Eds.), Inorganic Mass Spectrometry: Fundamentals and Applications, Marcel Dekker, New York, 2000, pp. 159–221.
[19] O. Gebhardt, Fresenius J. Anal. Chem. 365 (1999) 117.
[20] R.L. Gherna, in: P. Gerhardt (Ed.), Manual of Methods for General Microbiology, American Society for Microbiology, Washington, 1981.
[21] H.W. Nesbitt, D. Banerjee, Am. Mineral. 83 (1998) 305.
[22] C. Plog, L. Wiedmann, A. Benninghoven, Surf. Sci. 67 (1977) 565.
[23] P. Linhardt, Mater. Sci. Forum 289–292 (1998) 1267.